Bonding of Histidine to Cerium Oxide

ARTICLE *in* THE JOURNAL OF PHYSICAL CHEMISTRY B · JULY 2013

Impact Factor: 3.3 · DOI: 10.1021/jp404385h · Source: PubMed

6 AUTHORS, INCLUDING:

Nataliya Tsud
Charles University in Prague
107 PUBLICATIONS **1,042** CITATIONS
SEE PROFILE

Robert G Acres
Australian Synchrotron
26 PUBLICATIONS **214** CITATIONS
SEE PROFILE

Daniel Mazur
Charles University in Prague
19 PUBLICATIONS **102** CITATIONS
SEE PROFILE

Kevin Charles Prince
Sincrotrone Trieste S.C.p.A.
479 PUBLICATIONS **7,038** CITATIONS
SEE PROFILE

THE JOURNAL OF PHYSICAL CHEMISTRY B

Article

pubs.acs.org/JPCB

Bonding of Histidine to Cerium Oxide

Nataliya Tsud,*[,†] Robert G. Acres,[‡] Marianna Iakhnenko,[§] Daniel Mazur,[†] Kevin C. Prince,[‡,∥] and Vladimír Matolín[†]

[†]Charles University, Faculty of Mathematics and Physics, Department of Surface and Plasma Science, V Holešovičkách 2, Prague, 18000, Czech Republic

[‡]Elettra-Sincrotrone Trieste S.C.p.A., in Area Science Park, Strada Statale 14, km 163.5, Basovizza (Trieste), 34149, Italy

[§]Taras Shevchenko National University of Kyiv, Faculty of Physics, Department of Experimental Physics, 64, Volodymyrs'ka St., 01601 Kyiv, Ukraine

[∥]CNR-IOM Laboratorio TASC, Basovizza (Trieste), 34149, Italy

Supporting Information

ABSTRACT: Adsorption of histidine on cerium oxide model surfaces was investigated by synchrotron radiation photoemission, resonant photoemission, and near edge X-ray absorption fine structure spectroscopies. Histidine was evaporated in a vacuum onto ordered stoichiometric $CeO_2(111)$ and partially reduced $CeO_{1.9}$ thin films grown on Cu(111). Histidine binds to CeO_2 in anionic form via the carboxylate group and all three nitrogen atoms, with the imidazole ring parallel to the surface. The amino nitrogen atom of the imidazole ring (IM) is deprotonated, and both IM nitrogen atoms form strong bonds via π orbitals, while the α-amino nitrogen interacts with the oxide via its hydrogen atoms. In the case of $CeO_{1.9}$, the deprotonation of the amino nitrogen of the imidazole ring is less pronounced and N K-edge spectra do not show a clear orientation of the ring with respect to the surface. A minor reduction of the cerium surface on adsorption of histidine was observed and explained by charge exchange as a result of hybridization of the π orbitals of the IM ring with the f and d orbitals of ceria. Knowledge of histidine adsorption on the cerium oxide surface can be used for design of mediator-less biosensors where the histidine-containing proteins can be strongly bound to the oxide surface via the imidazole side chain of this residue.

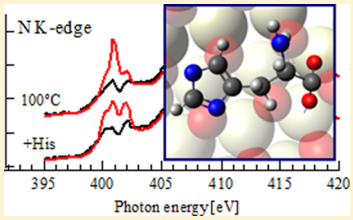

INTRODUCTION

Nanostructured metal oxides have recently aroused much interest as immobilizing matrixes for biosensor development. Oxides such as TiO_2, SnO_2, Fe_3O_4, CuO, and CeO_2 have been found to exhibit interesting nanomorphological, biocompatible, nontoxic, and catalytic properties. Some of these materials also exhibit enhanced electron-transfer kinetics and a strong adsorption capacity, thus providing suitable microenvironments for the immobilization of biomolecules and resulting in improved biosensing characteristics.[1−3]

To fabricate an efficient biosensor, it is crucial to select a nanostructured metal oxide that is suitable for immobilization of the desired biomolecules. The interface formed between oxide nanoparticles and biomolecules is known to critically affect the performance of a biosensor. The formation and properties of a nanobio interface depend on the nature of the oxide.[2,3] Among the important parameters are the effective surface area, surface charge, energy, roughness, valence/conduction states, functional groups, and physical and hydrophilic/hydrophobic characteristics. An effective metal oxide bio interface can help a biomolecule retain its biological activity with high stability by establishing a biocompatible microenvironment. There is, therefore, a considerable opportunity for the development of biosensors with improved sensitivity and detection limits, as well as lower cost and extended lifetime, through the use of suitable metal oxides.

Among the various metal oxides, cerium oxide has some unique properties, which make it a promising candidate for a biocompatible layer for electrochemical biosensing devices. Cerium oxide (CeO_2 or its non-stoichiometric forms) represents an active support for catalytic metals, alloys, or biomolecules which efficiently interact to achieve the desired chemical behavior in three-way automotive catalysts, solid-oxide fuel cells, and biosensors.[2−4] CeO_2 is known for its oxygen storage capacity, i.e., the ability to release a part of its oxygen content by varying its stoichiometry to provide oxygen to a reaction in its surroundings when the oxygen activity is low, while reabsorbing oxygen when the activity is high.[4−12]

Over the past few years, CeO_2 model systems have been widely investigated and characterized with regard to the interaction with adsorbed metal atoms and the chemical reactivity of simple gases (for example, CO_2 and O_2)[5,6,9,11] and small organic molecules (methane, ethylene, methanol).[7,8,10]

We report a study of the adsorption of histidine on a cerium oxide model support, by surface science techniques with the use of synchrotron radiation. As the nanostructured ceria films or powders for real bio sensing systems contain small crystallites of CeO_2 and Ce^{3+} sites adjacent to oxygen vacancies and at

Received: May 3, 2013
Revised: June 27, 2013
Published: July 2, 2013

   dx.doi.org/10.1021/jp404385h | J. Phys. Chem. B 2013, 117, 9182−9193

grain edges and other defects, ordered stoichiometric and partially reduced cerium oxide thin films were chosen as model supports. Histidine molecules were deposited on $CeO_2(111)$ and CeO_{2-x} grown on Cu(111) by Ce evaporation in an oxygen atmosphere. The chemical state, coverage, and bonding of the molecules were studied by synchrotron radiation photoelectron spectroscopy (SRPES) and resonant photoelectron spectroscopy (RPES); molecular orientation was examined by near edge X-ray absorption fine structure spectroscopy (NEXAFS). In view of the importance of nanostructured cerium oxide in various biological and recently also pharmacological applications,[13−17] the primary objective of this work is to investigate the basic properties of cerium oxide films in their bonding with the amino acid histidine.

Histidine was chosen because of its importance in various biological processes,[18] with the aim to model the bonding of proteins and other complex biomolecules with the cerium oxide surface. The structure of the histidine molecule is shown in Figure 1, and it has three important chemical groups: carboxylic acid, α-amino, and imidazole.

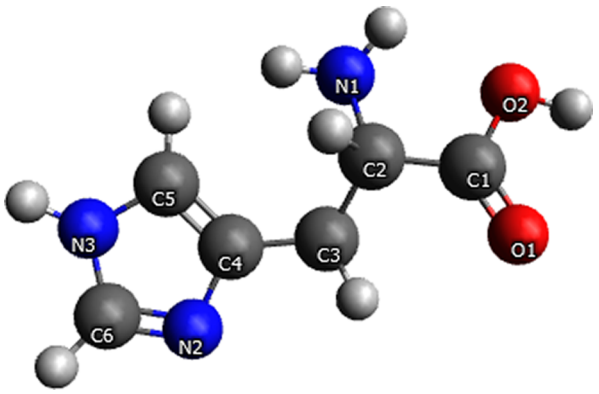

Figure 1. Schematic structure of histidine ($C_6H_9N_3O_2$).

A related model system is histidine adsorbed on metal surfaces.[19−23] For vacuum evaporation and deposition from a neutral solution of histidine on Au(111), an anionic adlayer of molecules was formed and bound to the surface via carboxylate and imidazole groups without α-amino group participation.[19] Histidine deposited from acidic solution on Au(111) and Au(110) results in the formation of a disordered adlayer because of the presence of the neutral carboxylic acid group together with the strongly interacting carboxylate group COO^-.[21] In all cases, the imidazole ring was found to be oriented at a shallow angle to the surface interacting via the imino nitrogen, with the α-amino group roughly perpendicular to the surface. These findings were recently confirmed by a molecular dynamics study of Xu et al.[22] Strong ionic−covalent bonding accompanied by a positive charge transfer to the substrate was found by Zubavichus et al. for histidine evaporated on polycrystalline gold foils.[23]

Another model substrate is a Cu(110) single crystal. At submonolayer coverage, histidine interacts with Cu(110) via the carboxylate group and imino nitrogen of the imidazole ring.[18,20] Annealing to 150 °C or preadsorption of oxygen induces additional histidine bonding with the copper surface via dehydrogenated amino nitrogen atoms of the ring and the amino side group.[20]

To our knowledge, there is no publication on histidine adsorption on well-defined bulk oxide surfaces. Many studies have been devoted to adsorption of other amino acids (proline, glycine, L-cysteine, etc.) on stoichiometric and reduced titanium dioxide surfaces.[24−26] It was shown that proline and glycine adsorb on TiO_2 surfaces via deprotonated carboxylate groups with a considerable contribution of zwitterionic species.[24,25] The proline zwitterionic concentration increases as the surface oxygen atom concentration decreases, i.e., on the reduced surface. Moreover, the reduced surface was shown to be partially reoxidized upon adsorption of proline.[24] The adsorption of alanine on the nonpolar ZnO(10−10) single crystal surface was studied by Gao et al.[27] A deprotonated alanine adlayer was observed at 25 °C bound to the surface via the carboxylate group. The thermal treatment of this adlayer was accompanied by decomposition and/or reaction on the surface. It was shown that the COO^- carboxylate group preferentially reacts with the surface at elevated temperature.

These studies explored the reaction of amino acids with relatively unreactive side chains, namely, hydrogen (glycine), methyl (alanine), and pyrrolidine (proline). In histidine, the imidazole side chain is more reactive, with important biological consequences, and in particular, it is polar and basic. This poses the question of whether the adsorption behavior is strongly influenced by these chemical differences in the side chain.

EXPERIMENTAL SECTION

The experiments were performed at the Materials Science Beamline at the Elettra synchrotron light source in Trieste, Italy. The beamline is based on a plane grating monochromator providing narrow band synchrotron light in the energy range 21−1000 eV. The experimental station is equipped with a Specs Phoibos 150 hemispherical electron energy analyzer, low energy electron diffraction (LEED) optics, a dual-anode Mg/Al X-ray source, an ion gun, a gas inlet system, a Ce evaporator, and a sample manipulator with a K-type thermocouple attached to the rear side of the sample. The base pressure in the chamber was below 3×10^{-10} mbar.

The epitaxial cerium oxide thin film was grown on a Cu(111) single crystal substrate. Cerium (Goodfellow, 99.99%) was evaporated in an oxygen atmosphere (5×10^{-7} mbar) onto Cu(111) at 250 °C, followed by annealing of the film at 250 °C in an oxygen atmosphere at the same pressure for 10 min. This procedure yields a stoichiometric (1.5 × 1.5) CeO_2/Cu(111) film. The oxide thickness was calculated from the attenuation of the Cu $2p_{3/2}$ core level intensity and was 15−18 Å, corresponding to 5−6 O−Ce−O layers of cerium oxide.[7,8] According to scanning tunneling microscopy studies, flat $CeO_2(111)$ terraces are separated by steps with a minor amount of Ce^{3+} centers on the step edges.[12] The Cu(111) crystal (MaTecK GmbH, 8 mm diameter, 2 mm thickness, 99.999%) was cleaned by several cycles of Ar ion sputtering and annealing to 450 °C. The surface cleanliness was checked by monitoring C 1s and O 1s photoelectron signals; no impurities were detected on the Cu(111) surface with sharp (1 × 1) LEED pattern before oxide deposition.

Partially reduced ceria film (CeO_{2-x}) was prepared by depositing 0.7 ML Ce metal on the stoichiometric $CeO_2(111)$ film at 250 °C, followed by flashing to 300 °C in a vacuum. The procedure yields a CeO_2 film covered by extended patches of the reduced CeO_{2-x}.[28] The index x was estimated on the base of analysis and fitting of the Ce 3d core level[9] and found to be 0.10.

L-Histidine $C_6H_9N_3O_2$ (≥99.5%) was supplied by Sigma-Aldrich and used without further purification. The evaporator

dx.doi.org/10.1021/jp404385h | J. Phys. Chem. B 2013, 117, 9182−9193

Table 1. Histidine Adlayer Thickness for As-Deposited Samples (25 °C) and after Flashing to 100 °C

	temp	(1) CeO_2	(2) CeO_2	(3) CeO_2	$CeO_{1.9}$	Cu
Cu $2p_{3/2}$	25 °C	24.0 Å	9.8 Å	1.5 Å	5.0 Å	
(1486.6 eV)	100 °C	20.0 Å	7.4 Å	1.6 Å	4.4 Å	4.2 Å
sample name		4 ML	2 ML	1 ML	1 ML	1 ML
		His/CeO_2	His/CeO_2	His/CeO_2	His/$CeO_{1.9}$	His/Cu

was inserted in a separate preparation chamber with a base pressure below 1×10^{-9} mbar (mainly water). Histidine was deposited by evaporation from a homemade Knudsen cell in a vacuum. Before deposition, the histidine powder in the crucible was degassed in a vacuum at 120 °C and then dosed at 135−140 °C onto the substrate at 25 °C. The deposition rate was about 1 monolayer (ML) per 300 s, determined from analysis of the photoemission data. The local pressure during deposition was about 3×10^{-8} mbar. The CeO_{2-x}/Cu(111) with $x = 0$, 0.1 or Cu(111) substrates, after preparation in the experimental chamber, were transferred to the preparation chamber for molecular deposition.

The C 1s, N 1s, and O 1s core levels were acquired with a photon energy of 410, 475, and 630 eV and a total resolution of 350, 500, and 700 meV, respectively. The valence band spectra were recorded at 43 (corresponding to the highest cross section for the adsorbate molecular orbitals), 115, 121.4, and 124.8 eV (to monitor Ce 4d → 4f resonances in Ce ions), with a total resolution of 190 meV measured as the width of the Fermi edge. The valence band spectrum measured at a photon energy of 115 eV corresponds to off resonance for the Ce^{3+} and Ce^{4+} states and was used as a reference for intensity subtraction between the corresponding features on- and off-resonance. Valence band spectra measured at 121.4 and 124.8 eV correspond to the D(Ce^{3+}) and D(Ce^{4+}) resonant enhancements in Ce^{3+} ion (emission from Ce 4f states located at a binding energy of about 1.4 eV) and Ce^{4+} ion (emission from hybridized oxygen cerium states at about 4.0 eV), respectively. The D(Ce^{3+})/D(Ce^{4+}) resonant enhancement ratio (RER) gives direct information about the oxidation state of surface cerium ions.[7,8,10] Al Kα radiation (1486.6 eV) was used to measure the core levels of C 1s, N 1s, O 1s, Ce 3d, and Cu $2p_{3/2}$, with a total resolution of 1 eV. The emission angle for the photoelectrons was 0 and 20° with respect to the sample normal for synchrotron light and the X-ray source, respectively. The intensity of the photoelectron spectra measured with synchrotron radiation was normalized to the incident photon flux. The core level spectra were fitted with Voigt or Gaussian profiles after Shirley background subtraction. The precision of the photon energy settings was verified by measuring the Fermi edge. All photoemission data were processed using the KolXPD fitting software.[29]

Checks for radiation damage were done by monitoring the C 1s core level spectra. No spectral changes were observed during one experimental step, i.e., stable signal for about 30 min. For the next experimental step, the analyzed point was changed on the sample surface. The homogeneity of the O 1s signal was checked before adsorption of histidine. Thus, the molecular adlayers were stable under our experimental conditions.

The NEXAFS spectra were taken at the C and N K-edges using the carbon and nitrogen KVV Auger yield, at normal (NI, 90°) and grazing (GI, 10°) incidence of the photon beam with respect to the surface. The energy resolution for the C and N K-edge NEXAFS spectra was estimated to be 0.23 and 0.38 eV, respectively. The polarization of light from the beamline has not been measured but is believed to be between 80 and 90% linear, as the source is a bending magnet. The raw NEXAFS spectra were normalized to the intensity of the photon beam, measured for the N K-edge by means of a high transmission gold mesh (simultaneously with the sample measurement) and for the C K-edge on a Au foil as the Au 4f intensity scanned after the sample (the gold sample was used because of interference of the carbon contamination on the gold mesh in the reference photon intensity spectrum). Then, the corresponding background spectra of the clean sample recorded under identical conditions were subtracted.

The coverage of histidine was estimated using the parametrized inelastic mean free path for organic materials:[30]

$$\lambda_m = 49/E_k^2 + 0.11E_k^{1/2}\ \mathrm{mg/m^2} \quad (1)$$

where E_k is the kinetic energy of photoelectrons. The λ_m value was converted to distances by dividing by the density of histidine powder[31] (1.42×10^9 mg/m^3). The inelastic mean free path for Cu $2p_{3/2}$ (excited by 1486.6 eV photons) photoelectrons passing through the histidine adlayer was found to be 18.2 Å. Using this value, the effective thickness of histidine on different substrates was calculated from the equation

$$I_d = I_0 \exp(-\lambda_m/d) \quad (2)$$

where I_d and I_0 are the attenuated and clean surface intensity of the photoelectron signal and d is the thickness of the molecular adlayer. The effective thickness d is calculated within a continuum model of the molecular film, and it has only qualitative character, as the actual morphology is not known.

RESULTS AND DISCUSSION

1. Molecular Adlayer Thickness Estimation and Sample Definition. The Cu $2p_{3/2}$ core level was used to determine adlayer thickness by measuring the attenuation of the signal after deposition. Three classes of samples were examined, namely, epitaxial stoichiometric CeO_2(111)/Cu(111), reduced $CeO_{1.9}$/Cu(111), and Cu(111). Histidine was deposited onto substrates at 25 °C, and then, the thermal stability of the adlayer was investigated from 100 to 300 °C in 50 °C steps. The values of thickness were calculated using eqs 1 and 2 and are shown in Table 1. For the first two substrates, we found multilayer coverage: about 4 ML for the sample designated (1) CeO_2 (evaporation at 140 °C for 15 min) and about 2 ML for sample (2) CeO_2 (135 °C, 10 min) which were stable against flashing to 100 and 150 °C. The number of monolayers has only qualitative character as a unit, and was determined under the assumption of layer by layer growth from the effective thickness of the layer. As monolayer coverage, we consider a saturated coverage of molecules adsorbed on the surface under certain experimental conditions without traces of the zwitterionic phase formation. Without knowledge of the orientation of the molecule, it is not a precise unit. However, below we will present data which sheds some light on the orientation, and allows the monolayer to be defined more

dx.doi.org/10.1021/jp404385h | J. Phys. Chem. B 2013, 117, 9182−9193

precisely. For (3) CeO_2, $CeO_{1.9}$, and Cu substrates (135 °C, 5 min), the calculated values were found to correspond to 1 ML histidine coverage (see further discussion). The thickness of 1 ML histidine is 4.40 Å on $CeO_{1.9}$ and 4.16 Å on Cu(111), and these are reasonable values considering the size of the molecule (the cube root of the molecular volume of histidine is 5.7 Å[19]). A much smaller number, 1.65 Å, was found for the (3) CeO_2(111) substrate which points to a different morphology upon histidine adsorption.

It is worth noting that by flashing to 150 °C the multilayer coverage, i.e., desorption of weakly bonded molecules, we did not get 1 ML coverage. Apparently, in the case of 2 or 4 ML histidine adlayers on the CeO_2 surface, heating to 100 or 150 °C results in the formation of a stable multilayer molecular film owing to strong intermolecular bonds.

The C 1s and N 1s core level spectra for 1, 2, and 4 ML of histidine on the CeO_2/Cu(111) substrate are shown in Figure 2. The kinetic energy of photoelectrons was 124 and 75 eV for

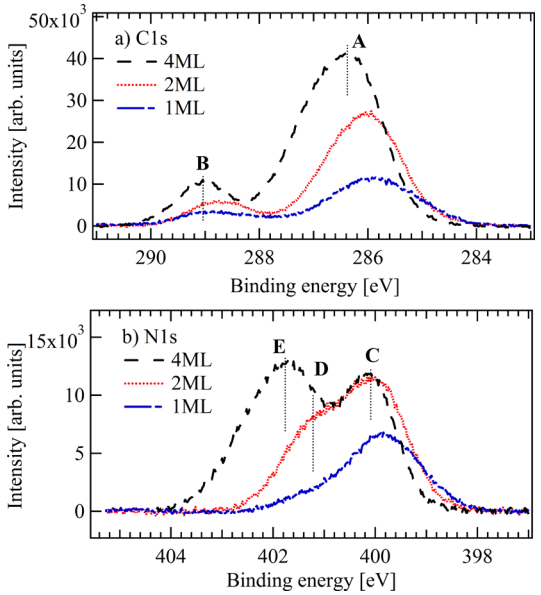

Figure 2. C 1s and N 1s core level spectra of histidine adlayers on the CeO_2/Cu(111) substrate after flashing to 100 °C. Photon energy 410 eV (C 1s) and 475 eV (N 1s).

C 1s and N 1s, respectively, corresponding to extremely surface sensitive conditions. This fact can explain the lower than expected absolute intensity for the 4 ML histidine adlayer on the ceria surface. Two well-separated peaks A and B in the C 1s core level spectrum were found with a shift to lower binding energy (BE) by 0.4 eV between data for 4 and 1 ML histidine coverage. The component B was assigned to carbon in the carboxylate COO^- group with a possible contribution of the neutral carboxylic group for coverage higher than 1 ML.[21] Component A accounts for the five other carbons of histidine.[19−21,23] The intensity ratio of B:A was found to be 1:(5.40 ± 0.15), which is in reasonably good agreement with the theoretical 1:5 value and other experimental work.[19,20] The carbon component ratio demonstrates that the structure of the histidine molecule is intact. The C 1s components' shift to lower binding energy by 0.4 eV as the coverage decreases is in line with previously published work on related systems.[19,20,23]

The N 1s core level spectra have different shapes for 1, 2, and 4 ML histidine coverage. Three components C, D, and E can be distinguished which were assigned to the imino and amino nitrogen atoms and nitrogen of the zwitterion histidine species, respectively.[19−21,23] The presence of the zwitterion phase is a typical feature for the multilayer coverage. Because of strong bonding with the cerium oxide surface at 1 ML coverage, the D:C components' intensity ratio does not correspond to the expected 2:1 for histidine but has a value of 1:(2.30 ± 0.10) after histidine adsorption. The components of the C 1s and N 1s spectra and their positions will be further discussed in detail below.

The integrity of the histidine molecules after evaporation in a vacuum and adsorption on the surface was checked again for the highest coverage, 4 ML His/CeO_2, i.e., the sample with strong signals of C 1s, N 1s, and O 1s, measured with 1486.6 eV photon energy. All signals were found to be stable. The ratio of peak intensity C:N:O divided by the corresponding photoionization cross sections was found to be (3.20 ± 0.10):(1.54 ± 0.10):1, in good agreement with the theoretical value 3:1.5:1.

The Ce 3d core level spectra of clean ceria substrates are shown in Figure 3a. The spectral structure corresponds well to stoichiometric and partially reduced cerium oxide: three doublets V−U, V″−U″, and V‴−U‴ for Ce^{4+} ions in CeO_2 and two additional doublets V_0−U_0 and V′−U′ (five in total) appear for Ce^{3+} ions in $CeO_{1.9}$.[7,8,10] The electronic structure of

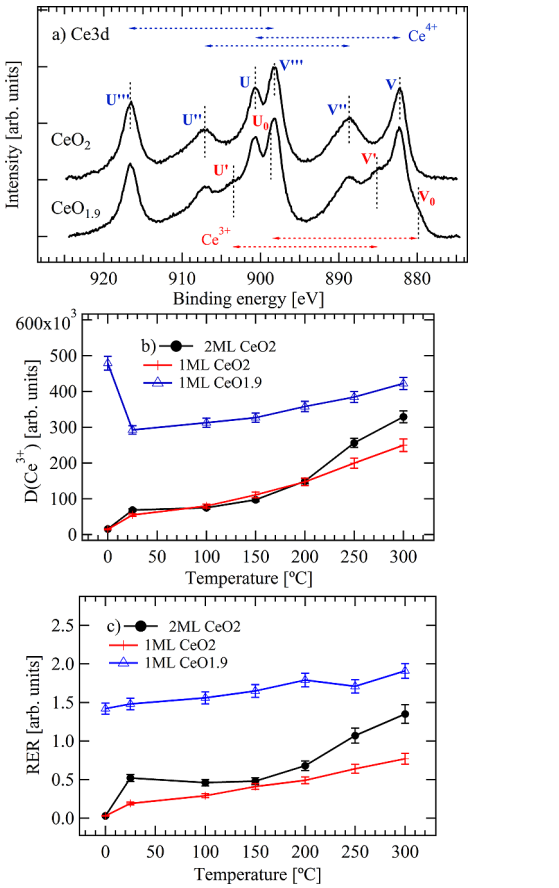

Figure 3. (a) Ce 3d core level spectra of the stoichiometric CeO_2/Cu(111) and reduced $CeO_{1.9}$/Cu(111) oxide, photon energy 1486.6 eV; (b) D(Ce^{3+}) intensity; (c) resonance enhanced ratio D(Ce^{3+})/D(Ce^{4+}) versus annealing temperature of histidine adlayers on cerium oxides. Values at 0 °C correspond to clean surfaces. The Ce 3d spectrum for $CeO_{1.9}$ is shifted by 0.5 eV to the low BE side.

dx.doi.org/10.1021/jp404385h | J. Phys. Chem. B 2013, 117, 9182−9193

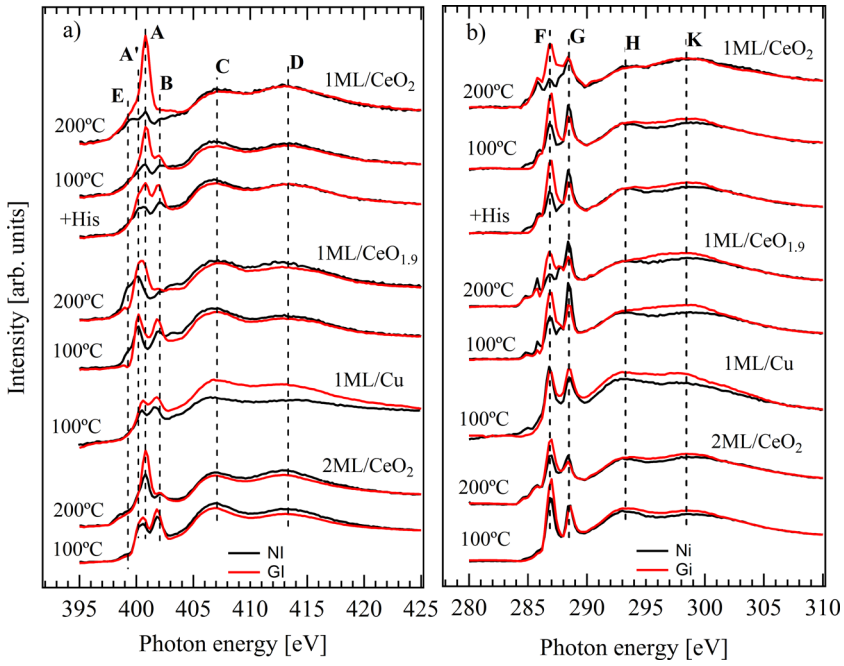

Figure 4. N K-edge (a) and C K-edge (b) NEXAFS spectra at temperatures indicated, at grazing (GI) and normal incidence (NI).

Table 2. NEXAFS Spectral Features in the π^* Resonance Range and Their Assignment

	N K-edge			C K-edge	
	E (eV)	**A** (**A′**) (eV)	**B** (eV)	**F** (eV)	**G** (eV)
assignment	1s → π^*	1s → π^*	1s → π^*	1s → π^*	1s → π^*
		IM imino N	IM amino N	IM ring	COO^-
1 ML His/CeO_2					
+His		400.8 (400.2)	402.0	287.0	288.5
100 °C		400.9	402.0	287.0	288.5
200 °C	399.2	400.8		286.8	288.4
1 ML His/$CeO_{1.9}$					
100 °C	399.2	(400.2)	401.9	286.9	288.5
200 °C	399.2	400.4		286.8	288.5
1 ML His/Cu					
100 °C		400.6	401.8	286.8	288.5
2 ML His/CeO_2					
100 °C		400.7 (400.2)	401.8	286.9	288.5
200 °C	399.0	400.8	402.0	286.9	288.5
1 ML His/Cu(110)[20]					
25 °C		399.5	401.2		
150 °C		400.0	401.2		
0.4 ML His/O−Cu(110)[20]		400.2	401.2		
1 ML His/Au(111)[19]		399.9	401.35		
His/Au(111) (110) acidic solution[21]		400.1	401.5		
His, powder[32]		399.8	401.3	286.8	288.6
His, ab initio[33]				288.72	292.12
				288.82	
				289.16	
His, thin film[35]				286.5	288.7
				287.0	
solid state IM[34]		400.4	401.8	286.5	

CeO_2 is characterized by unoccupied 4f states of Ce^{4+} cations ($4f^0$), while Ce_2O_3 consists of Ce^{3+} cations with ($4f^1$) configuration. The Ce 3d doublets represent different 4f configurations in the photoemission final state due to Ce 4f occupation in the initial and final states.

Except for a decrease of intensity, no change in the Ce 3d core levels on histidine adsorption was observed because of the low resolution and large information depth for photoelectrons excited by Al Kα radiation. An example of the Ce 3d core level spectra of the stoichiometric CeO_2/Cu(111) oxide before and after histidine adsorption and subsequent annealing is given in

dx.doi.org/10.1021/jp404385h | J. Phys. Chem. B 2013, 117, 9182−9193

the Supporting Information. Therefore, the surface oxidation/reduction character was tracked by following the behavior of the valence band resonances connected with Ce^{3+} and Ce^{4+} states. The RER resonance ratio was about 0 for CeO_2 and 1.4 for $CeO_{1.9}$ before histidine adsorption (Figure 3c). A slight increase of the RER ratio with temperature was observed for both types of oxide, i.e., stoichiometric and reduced (see Figure 3c).

Because of the bulk nature of the Ce^{4+} cations, the associated resonance peak is attenuated by histidine more than that of the Ce^{3+} peak, which originates from Ce^{3+} ions on the surface, so we focus attention on the $D(Ce^{3+})$ dependence alone. The almost identical $D(Ce^{3+})$ behavior for histidine adlayers on CeO_2 and $CeO_{1.9}$ indicates an increase of the Ce^{3+} ion concentration independent of the initial degree of surface reduction. The increase of Ce^{3+} concentration can be tentatively attributed to charge transfer from the molecule to the substrate rather than oxygen desorption which requires much higher temperature treatment (675 °C).[12] This hypothesis will be further discussed in the text.

For the reduced oxide surface, a rigid shift of ceria and histidine photoemission peaks of 0.35 ± 0.15 eV to high binding energy was observed. We explain this shift by a difference in the Fermi level pinning between the stoichiometric and reduced cerium oxide, and it is not related to electronic structure changes of the interface with the molecules. To compensate for this change of reference level, and allow spectra from different surfaces to be compared, all spectra measured on the reduced surface were adjusted by the values indicated in the figures, which moves them to lower binding energy.

2. NEXAFS Spectroscopy. The NEXAFS spectra of the histidine adlayers on CeO_2, $CeO_{1.9}$, and Cu(111) substrates measured at the indicated temperatures and geometries are shown in Figure 4.

Four prominent features were found in the N K-edge spectra marked A, B, C, and D (see Figure 4a). The sharp peaks A and B in the range 399−402 eV correspond to excitations of N 1s electrons of the IM ring transition to the lowest unoccupied molecular orbitals (LUMOs) with π^* character, i.e., 1s → π^* transitions for imino N2 (A) and amino N3 (B). The broad features C and D at 407.0 and 413.0 eV, respectively, were attributed to resonances of all three histidine nitrogen atoms of character 1s → σ^* (N−C). Such structured absorption spectra with π^* and σ^* resonance ranges are a common feature for the adlayers of molecules with unsaturated bonds.[19,20,32] For C K-edge spectra, the region of 1s → π^* transitions has rich structure with strong contributions of the feature F at 286.9 eV from the IM ring carbons and G at 288.4 eV from the carboxylate carbon.[32−34] In this case, the C 1s → σ^* resonances H and K are located at 293 and 298.7 eV. The energies of the observed π^* resonances in the N and C K-edge spectra and their assignment compared to the published data on the related substrates are shown in Table 2.

The N K-edge spectra of the 1 ML histidine adlayer on CeO_2 gave the best contrast between the two geometries, and this indicates molecular ordering on the surface. The ratio of π^* to σ^* resonance intensity is higher at GI geometry, which shows that the IM ring is almost parallel to the surface. The dipole moment of the π^* orbitals is oriented perpendicular to the IM ring, and when the molecule is adsorbed parallel to the surface, this feature has strong intensity (relative to σ^* resonances) at GI geometry. At NI geometry, the electric vector is parallel to the surface and induces transitions within the surface plane; i.e., the π^* resonances vanish for ideally parallel molecular adsorption. For the normal incidence spectra, the degree of polarization is not important because the electric vector is always parallel to the surface. Our conclusion is based on the observation that the π^* resonances do not disappear in this geometry, and hence the molecular plane is not perfectly parallel to the surface. At grazing incidence, it is true that elliptical light has a component parallel to the surface, but this does not excite the resonance.

This flat geometry explains the low value of the histidine thickness on CeO_2 (1.65 A, see Table 1). It can be seen that the structure of the π^* resonances changes with temperature. Right after deposition, three components were distinguished in the N K-edge 1s → π^* transitions region: A, A′, and B at photon energies of 400.8, 400.2, and 402.0 eV (see Table 2). The energy of the A, B, C, and D features is about 0.7−0.9 eV higher than in the case of histidine powder[32] and adlayers on Au(111) and Cu(110) surfaces.[19,20] The energy separation between A and B is 1.2 eV with about equal intensity right after histidine deposition. The closely related resonances A and A′ were attributed to the adsorption of the imidazole ring in two different environments with imino nitrogen strongly chemisorbed (A) and more weakly bound to the surface (A′).[20] Flashing to 100 °C considerably reduces the intensity of the A′ and B resonances, and is accompanied by significant growth of component A. The shift of A′ by 0.6 eV to higher energies indicates stronger bonding of the IM ring with the cerium oxide surface; a similar effect was observed for histidine adlayers on the Cu(110) surface.[20] Thus, the thermal treatment causes the strong chemisorption of the IM ring to the surface via imino N and deprotonation of the amino N together with possible desorption of weakly bound histidine molecules. Flashing to higher temperature reduces again the B resonances' intensity with significant growth of the A component. In other words, the IM ring binds to the cerium oxide surface via its two nitrogen atoms, imino N and deprotonated amino N; the ring is roughly parallel to the surface.

C K-edge NEXAFS spectra give similar results. The energy positions of peaks are equal within 0.4 eV to published data of polycrystalline histidine powder[32] and solid state imidazole.[34] C 1s → π^* resonances corresponding to the IM ring (component F) have very different intensity at GI and NI geometries. The changes with angle for the component G are less prominent and in the opposite direction; i.e., the ratio of π^* to σ^* resonances is higher at NI. We conclude that, for as-deposited histidine and histidine adlayers after flashing to 100 °C, the IM ring is lying close to the surface with the carboxylate group at a steep angle. Flashing to 200 °C increases the difference between π^* resonances for component F, while other features remain unchanged when comparing the two geometries. This confirms the previous conclusion that the IM ring is at a shallow angle to the oxide surface.

The N K-edge NEXAFS spectra of 1 ML histidine on the $CeO_{1.9}$ oxide differ substantially in both the shape of π resonances and their angular dependence. The absence of a strong angular dependence of the π^*/σ^* intensity ratio indicates random geometry of the IM ring, which is in line with the estimated thickness of 4.40 Å for ML histidine coverage on $CeO_{1.9}$. In general, the same four main resonances A, B, C, and D were found. The well-resolved features A′ and B with a small shoulder E were observed after flashing to 100 °C. With respect to the stoichiometric surface, shifts of the

dx.doi.org/10.1021/jp404385h | J. Phys. Chem. B 2013, 117, 9182−9193

component A to lower energy by 0.7 and 0.4 eV after flashes to 100 and 200 °C, respectively, were observed. Component B remained almost at the same energy and vanished above 200 °C, the same behavior as that for 1 ML histidine on CeO_2. Similarities in C 1s and N 1s spectra (see next section) may lead us to expect similar NEXAFS data, but for $CeO_{1.9}$, we definitely have the new feature E at low photon energy, at 399.2 eV; it is more pronounced at NI geometry. We speculate that the component E may be due to the α-amino nitrogen interacting with the oxide surface via a hydrogen bond. Traces of the component E can be found even for 1 ML histidine on CeO_2 (related to a low concentration of Ce^{3+} centers). After we have presented the photoemission spectra, this argument will be developed further in the discussion section.

The C K-edge spectra of 1 ML histidine on $CeO_{1.9}$ are very similar to those measured on CeO_2, pointing to partial orientation with the IM ring close to parallel to the surface, and the carboxylate group at a steep angle. The C K-edge feature at 285.8 eV which is more pronounced at NI geometry can be tentatively attributed to the C2 carbon, the carbon which is bound to N1.

The 2 ML histidine on the CeO_2 sample is characterized by absorption spectra similar to 1 ML coverage: well-separated features A and B after 100 °C flash and mainly component A after flashing to 200 °C. No clear angular dependence was observed in the N and C K-edge NEXAFS spectra, indicating that the molecules are randomly oriented.

The absorption spectra of 1 ML histidine on Cu(111) after flashing to 100 °C have the strong features A and B in the N K-edge spectra, attributed to imino and amino nitrogen atoms of the IM ring, and F and G in the C K-edge due to carbon atoms of the IM ring and COO^- group, respectively. The A and B resonances are shifted to lower energy by 0.2 eV with respect to the oxide surface, and have the same energy separation of 1.2 eV. No change in the spectra with angle of incidence of the light was observed, indicating random histidine orientation on Cu(111), which is consistent with the ML thickness value of 4.16 Å.

3. Photoemission Spectroscopy. The O 1s spectra (Figure 5) of the oxide substrates are dominated by a peak at 529.6 eV, which is associated with the O^{2-} anions located near Ce^{4+} centers on CeO_2. An additional small peak at 532 eV is assigned to $O^{2-}(Ce^{3+})$ anions on $CeO_{1.9}$ with some

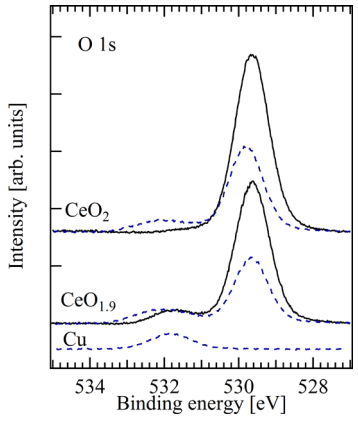

Figure 5. O 1s core level spectra, photon energy 630 eV. Black lines, signal from clean substrates; dashed blue lines, signals from 1 ML histidine overlayer on the corresponding substrate. The data for $CeO_{1.9}$ is shifted by 0.33 eV to lower BE.

contribution of adsorbed OH groups. The lattice oxygen peak is attenuated after histidine adsorption and a small new component appears at about 532.1 eV assigned to carboxylate oxygen. For reference, on Cu(111), the carboxylate oxygen was found at 531.80 eV. These values are in good agreement with the published values for the COO^- group of alanine on ZnO (531.7 eV),[27] proline on TiO_2(110) (532.3 eV),[24] and bi-isonicotinic acid on TiO_2(110) (531.7 eV).[36] No O 1s signal was observed at 533 eV or higher binding energy, which is the signature of the protonated COOH group.[36] Moreover, considering the C 1s core level spectra, see further discussion, the presence of the carboxylic COOH oxygen can be excluded. The single COO^- component is clearly visible on CeO_2 and Cu(111). On $CeO_{1.9}$, it contributes to the original $O^{2-}(Ce^{3+})$ peak as a shoulder at high BE. The single adsorbate component indicates the same chemical state for two carboxylate oxygens, i.e., anionic bonding of histidine via the COO^- group according to the equation

$$\mathrm{His(COOH)_g + O_s \rightarrow His(COO^-)_a + (OH)_s} \quad (3)$$

where the indices g and a stand for gaseous and adsorbed histidine. The dissociated proton binds to a surface oxygen O_s, forming a surface hydroxyl group $(OH)_s$. Because of the low intensity and the similar O 1s binding energy of the adsorbed hydroxyl group on cerium oxide (531.0–532.0 eV[37]), we cannot distinguish it from COO^- in the peak at 532 eV.

The N 1s core level spectra of the 1 ML histidine adlayer on CeO_2, $CeO_{1.9}$, and Cu and 2 ML on CeO_2 are shown in Figure 6. N 1s spectra were fitted with 2 or 3 Gaussian components with equal width and BE values shown in Table 3. As already mentioned in section 1, the components C, D, and E were assigned to the imino and amino nitrogen atoms and nitrogen of the zwitterion histidine species. The neutral histidine molecule has 1 imino nitrogen (N2) and two amino nitrogen atoms (N1 and N3), which have similar binding energies. Thus, we expect for the neutral molecule the ratio of N 1s components to be 2:1. Instead, for 1 ML histidine on CeO_2 (25 °C), $CeO_{1.9}$ (25 °C), and Cu (100 °C) substrates, we measured D:C = 1:(2.20 ± 0.10), corresponding to one amino and two imino-like nitrogen atoms. We recall the NEXAFS data from the previous section, where we have shown that there are π^* resonances from two different nitrogen atoms (imino and amino) of the IM ring of histidine on all substrates. Thus, in N 1s photoemission spectra, we expect to distinguish them very well and component D has been assigned mainly to the amino nitrogen of the IM ring (N3). Component C therefore accounts for two other nitrogen atoms, originally the imino N2 atom and amino N1 atom, with N1 shifted to lower BE due to interaction with the substrate. Most likely N1 amino nitrogen binds with $O^{2-}(Ce^{3+})$ anions via hydrogen; see further discussion. Such an effect of an amino group bonding via hydrogen atoms was observed on glycyl–glycine adsorption on Cu(110) and was confirmed by theoretical calculations.[38] It would seem to be unfavorable for the N1 atom to lose both of its protons and then interact with the substrate. Acid–base bonding will also affect the binding energy of the C2 and C3 atoms. The imino N2 atoms that are weakly and strongly bound to the CeO_2 surface (which correspond to A and A′ components in NEXAFS spectra) apparently have similar binding energies, and we are not able to resolve them.

With increasing temperature, the intensity of component D gradually decreases, contributing to component C. The shift of intensity from D to C is interpreted as deprotonation of the

dx.doi.org/10.1021/jp404385h | J. Phys. Chem. B 2013, 117, 9182–9193

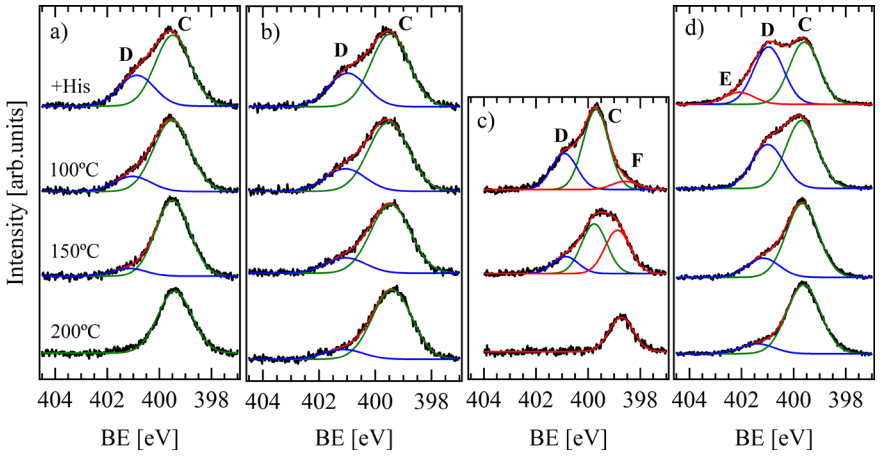

Figure 6. N 1s core level spectra, photon energy 475 eV: (a) 1 ML His/CeO_2; (b) 1 ML His/$CeO_{1.9}$; (c) 1 ML His/Cu(111); (d) 2 ML His/CeO_2. The data for $CeO_{1.9}$ is shifted by 0.25 eV to lower BE.

Table 3. Binding Energies (eV) of N 1s Core Level Components Compared with Published Data

	D	C	F
	amino N	imino N	N-metal
2 ML His CeO_2, 100 °C	401.00	399.69	
1 ML His CeO_2, 100 °C	401.03	399.52	
1 ML His $CeO_{1.9}$, 100 °C	401.06	399.52	
1 ML His Cu(111), 100 °C	400.91	399.70	398.58
1 ML His gold[23]	400.9	399.5	
1 ML His Cu(110)[20]	400.55	399.60	398.60
1 ML His Au(111)[21]	400.67	399.47	398.77

amino N3 nitrogen atom following eq 4, which is in line with the NEXAFS results.

$$\mathrm{His}(C_3H_3N_2)(COO^-)_a + O_s \rightarrow \text{temperature} \rightarrow \mathrm{His}(C_3H_2N_2^-)(COO^-)_a + (OH)_s \quad (4)$$

where $C_3H_2N_2^-$ is an imidazole ring with deprotonated amino nitrogen atom. Again, the dissociated proton binds to a surface oxygen O_s, forming a surface hydroxyl group $(OH)_s$.

Thermal treatment therefore induces stronger bonding of histidine in the anionic form His^{2-} with the cerium oxide surface via the IM ring N3 atom, and is accompanied by the formation of surface OH groups. Comparison of changes in the D component area indicates N3 deprotonation is slower on the reduced oxide, implying the process is connected either with Ce^{4+} or $O^{2-}(Ce^{4+})$ centers on the surface, the concentration of which is lower for $CeO_{1.9}$.

We have shown that histidine binds to the cerium oxide surface via the imino N2 and α-amino N1 atoms immediately after adsorption at room temperature. Annealing of the histidine adlayer induces additional interaction via deprotonation of the N3 atom, which is enhanced on the stoichiometric oxide.

Similar behavior was observed for the 2 ML histidine adlayer on CeO_2 (see Figure 6d). Heating to 100 °C results in desorption of weakly bound zwitterionic species (component E in the N 1s spectrum). The C component corresponding to imino nitrogen atoms always dominates, while the component D again vanishes with increasing temperature. We conclude that the interfacial layer of histidine has the same nature (macroscopic qualities) for 1 and 2 ML coverage.

For 1 ML of histidine on Cu(111) after flashing to 100 °C, the new component F was found at binding energy 398.6 eV and was assigned to N−Cu strong bond formation.[20,21] The ratio of the other two components is similar to previous cases.

Heating of histidine overlayers on the cerium oxide and Cu(111) surfaces resulted in molecular decomposition and partial desorption starting from 200 °C. The N 1s peak intensity significantly decreased above 150 °C especially for the Cu(111) substrate (see Figure 7). Thus, the molecular stability of histidine on the oxide is much higher than that on the copper surface.

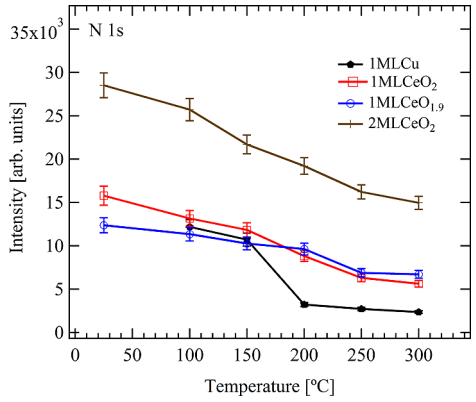

Figure 7. N 1s total intensity versus annealing temperature.

The C 1s core level spectra are shown in Figure 8. They were fitted with 4 Gaussian components with equal width, and BE values shown in Table 4. The total C 1s intensity (a) and the intensity of each single component for 1 ML His/CeO_2 (b) and 1 ML His/$CeO_{1.9}$ (c) versus annealing temperature are shown in Figure 9. The ratio of peak intensities of p4 to (p1+p2+p3) was found to be 1:(5.05 ± 0.25) for all samples after deposition and flashing to 100 °C, so we conclude that the molecule adsorbs intact with all six carbons. We are not aware of any gas phase measurements of histidine, but we can estimate the difference in 1s binding energy between the carboxylic acid carbon and the other carbon atoms in the following manner. Zhang et al.[39] have measured the spectra of a number of related aromatic amino acids, and the carboxylic acid C 1s binding energy is between 294.6 and 294.85 eV. Wickrama Arachchilage et al.[40] have measured the photoemission spectrum of a

dx.doi.org/10.1021/jp404385h | J. Phys. Chem. B 2013, 117, 9182−9193

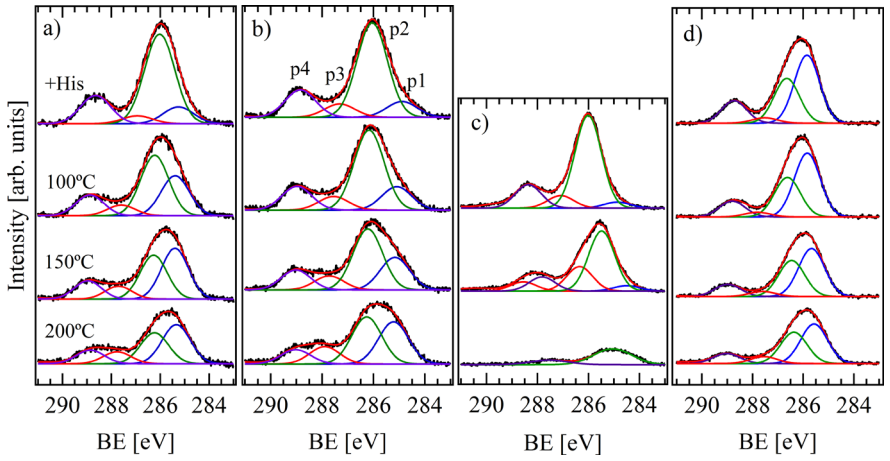

Figure 8. C 1s core level spectra, photon energy 410 eV: (a) 1 ML His/CeO_2; (b) 1 ML His/$CeO_{1.9}$; (c) 1 ML His/Cu(111); (d) 2 ML His/CeO_2. The data for $CeO_{1.9}$ is shifted by 0.39 eV to lower BE.

Table 4. Binding Energy Values for C 1s Core Level Components Compared with Published Data

	P1 (C3)	P2 (C4+C5+C6)	P3 (C2)	P4 (C1)
2 ML His CeO_2, 100 °C	285.70	286.48	287.81	288.66
1 ML His CeO_2, 100 °C	285.25	286.09	287.45	288.74
1 ML His $CeO_{1.9}$, 100 °C	284.95	286.03	287.41	288.84
1 ML His Cu, 100 °C	284.74	285.87	286.95	288.22
1 ML His Au(111)[19]	285.85 (120 °C) other carbon atoms			288.1 (120 °C), COO−
1 ML His Cu(110)[20]	285.10 (150 °C) other carbon atoms			288.1 (150 °C), COO−
glycine TiO_2(011)[25]			286.7 (25 °C), H_2N−CH_2	289.2 (25 °C), COO−
proline TiO_2(110)[24]	285.0 (25 °C), CH_x	286.2 (25 °C), CN		288.4 (25 °C), COO−
alanine ZnO(1010)[27]	285.4 (25 °C), $-CH_3$	286.7 (25 °C), $-HCR_2$		288.8 (25 °C), COO−

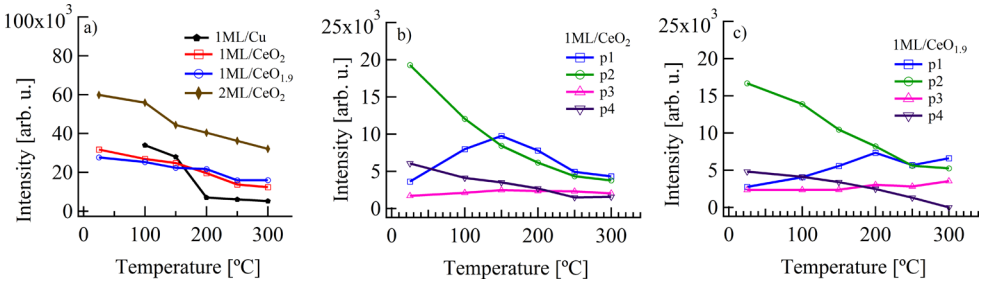

Figure 9. C 1s core level intensity for all substrates (a) and C 1s component intensity for 1 ML histidine on CeO_2 (b) and $CeO_{1.9}$ (c) surfaces versus annealing temperature.

histidine containing dipeptide, and the C 1s binding energies of the atoms in the imidazole side chain vary from 291.0 to 292.0 eV. The weighted average difference (two states contribute to the 292 eV feature) is 3.1 eV. The BE energy difference between the p4 component and the maximum of the broad peak is 2.2−2.8 eV, which is lower than this estimated value for histidine in the gas phase. This chemical shift is clearly due to chemisorption of histidine on the surfaces.

For 1 ML coverage, peak p3 appears almost immediately after histidine adsorption and it is more pronounced for the $CeO_{1.9}$ surface than for CeO_2. This component is assigned to C2 atoms and accounts for the α-amino N1 nitrogen bonding to cerium oxide. We suggest that N1 binds strongly to the oxide surface via two hydrogen atoms. The positive charge of hydrogen bonded to N1 implies bonding to surface oxygen atoms. On the other hand, the p3 components are more distinct on the reduced ceria, which has less surface oxygen, and the intensity is directly related to the concentration of the Ce^{3+} surface ions. Thus, we can expect N1(H_2) attraction to O^{2-}(Ce^{3+}) anions. The BE shift of the carboxylic carbon (p4) of about 0.5 eV is well visible in Figure 2a comparing 4 ML and 1 ML histidine adlayer on CeO_2. In Figure 8, we do not see such a shift because the carboxylic COOH group deprotonates immediately after histidine deposition. As for the p3 component of the C1s core level (Figure 8), it shifts also about 0.5 eV to higher BE. Thus, the BE shifts for these two carbon atoms are comparable. The difference in the bonding and resulting electron redistribution could explain the shift in opposite directions. The relative intensity of p3 is lower than p4 right after deposition and after flashing to 100 °C, while it is almost equal to p4 after heating to 150 °C. Taking into account that p4 is due to carboxylate carbon (with intensity corresponding to one carbon atom), we conclude that the

dx.doi.org/10.1021/jp404385h | J. Phys. Chem. B 2013, 117, 9182−9193

N1(H_2)−O^{2-}(Ce^{3+}) bonding develops with temperature and most likely depends on the Ce^{3+} cation surface concentration.

Two components were distinguished in the broad main peak centered at about 286 eV. According to the literature, p1 corresponds to C bonded only to C and H and is assigned to the C3 atom. p2 can be attributed to carbon atoms bonded to N in the IM ring. With increasing temperature, there is clear intensity redistribution between p1 and p2 (see Figure 9). The p1 component grows faster on the CeO_2 surface where the NEXAFS data showed the most parallel geometry for the histidine IM ring and bonding of both nitrogen atoms to the oxide. For the partially reduced $CeO_{1.9}$ surface, the growth of p1 is slow and can be connected with the reduced concentration of oxygen on the surface. We explain this observation as a mutual charge transfer between the histidine molecule and the oxide; i.e., some charge from π orbitals of the IM ring goes to unoccupied $4f^0$ orbitals of the Ce^{4+} cations, and it is compensated by the Ce 5d electron donation to the π orbitals of the IM ring as a result of orbital hybridization, as was suggested for water interaction with the cerium oxide surface in ref 41. It is directly connected with the increase of the Ce^{3+} centers ($4f^1$ configuration) on the surface and can explain the gradual development of the p3 component for 1 ML His/CeO_2. The $CeO_{1.9}$ surface has higher Ce^{3+} initial concentration, and the N1(H_2)−O^{2-}(Ce^{3+}) bonds form more readily. The charge transfer is in line with the amino N3 atom deprotonation (decreasing intensity of the component D in the N 1s spectra, together with vanishing of the component B in the N K-edge absorption spectra). The $CeO_{1.9}$ surface partially covered with Ce^{3+} ions is not so reactive. In this case, the deprotonation is suppressed and results in a smaller charge exchange.

We conclude that for CeO_2 all three N atoms are involved in the histidine bonding, with the IM ring parallel to the surface (which is confirmed by N K-edge NEXAFS spectra). The amino nitrogen atom of the IM ring is deprotonated and both IM nitrogen atoms form strong bonds via π orbitals, while the α-amino nitrogen interacts with the oxide via its hydrogen atoms. In the case of partially reduced $CeO_{1.9}$, the deprotonation of the amino N of the IM ring is less pronounced and N K-edge NEXAFS spectra do not show such clear dependence on the angle.

Valence band difference spectra (adsorbate-covered minus clean surface spectra) of samples after flashing to 100 °C are presented in Figure 10; the original spectra are shown in the Supporting Information. The spectra were measured with 43 eV photon energy, corresponding to the high cross section of the histidine molecular orbitals. Feature A was assigned to nonbonding molecular orbitals localized on the α-amino group N1 and imino nitrogen N2 as well as oxygen lone pairs. Peaks B and C are related to the molecular orbitals of π and σ symmetry, respectively, which are strongly delocalized in the IM ring plane.[20] For 1 ML histidine on CeO_2 and $CeO_{1.9}$, we do not see the features assigned to π and σ orbitals due to their low intensity or delocalization. Two ML histidine coverage is characterized by a similar interface with the oxide surface with the σ orbital feature shifted to lower BE with respect to 4 ML coverage. The small feature at 2.4 eV can be assigned to the 4f orbitals of cerium oxide filled by partial charge transfer from histidine, as was suggested for water interaction with the cerium oxide surface.[41] This feature is more pronounced for 1 ML histidine on CeO_2 and partially attenuated for 2 ML coverage. Apparently, interaction between π orbitals of the IM ring and f

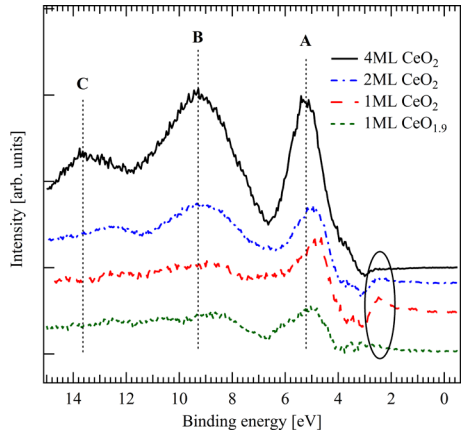

Figure 10. Valence band difference spectra of samples after flashing to 100 °C, 43 eV photon energy. The data for $CeO_{1.9}$ is shifted by 0.40 eV to lower BE.

and d orbitals of ceria results in mutual charge exchange, leading to occupation of the Ce $4f^1$(Ce^{3+}) states. This process is compensated by Ce 5d electron donation to histidine π orbitals due to their hybridization. The higher binding energy of 2.4 eV compared to 1.4 eV for normal Ce $4f^15d^16s^2$ (Ce^{3+}) states was explained by the less efficient screening of the f electrons in the Ce $4f^15d^06s^2$ configuration.[41]

The results described above can be combined to construct a model for the adsorption of histidine on the cerium oxide. We propose a model for the stoichiometric ordered CeO_2 film in Figure 11. As observed with NEXAFS spectra, the IM ring

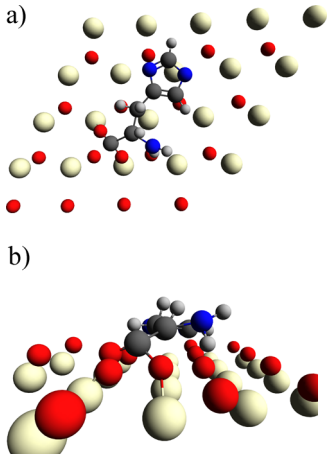

Figure 11. Adsorption model of histidine on the CeO_2 surface: (a) top view; (b) side view.

binds to the cerium oxide surface via its two nitrogen atoms, imino N and deprotonated amino N, and with the carboxylate group; the ring is roughly parallel to the surface. The photoemission results are in good agreement with these conclusions and provide further details on the histidine adsorption geometry. The N 1s core level with a single dominant component for 1 ML His/CeO_2 after flashing to 150 °C (Figure 6a) confirms the fact that all three nitrogen are involved in the strong bonding with the oxide. It was shown that the N1 α-amino nitrogen interacts with O^{2-}(Ce^{3+}) anions via hydrogen atoms. The IM ring π orbitals hybridized with the f and d orbitals of ceria and charge exchange takes place leading

dx.doi.org/10.1021/jp404385h | J. Phys. Chem. B 2013, 117, 9182−9193

to occupation of the Ce $4f^1(Ce^{3+})$ states and explaining the slight reduction of the cerium oxide.

We did not consider the dehydrogenation of the α-amino group of adsorbed histidine on the cerium oxide and further reaction of hydrogen with OH groups on the cerium oxide, which results in water formation and its desorption, but it cannot be completely ruled out. Water molecules partially dissociate on defects or step edge sites of cerium oxide at −110 °C, so only a limited amount of adsorbed OH groups are expected at room temperature on the reduced surface.[37] Indeed, they contribute to the O 1s component at 532 eV on $CeO_{1.9}$, while no intensity in this region was found on CeO_2. Additional OH groups appear as a result of histidine deprotonation and bonding in the His^{2-} anionic form. Thus, the effect of OH groups would be much more pronounced on the partially reduced $CeO_{1.9}$ surface, where their concentration is higher. Because of the low intensity, it was difficult to track the changes in the O 1s component at 532 eV with temperature increase. An alternative measure of the Ce^{3+} concentration is $D(Ce^{3+})$, the resonant intensity of the valence states (Figure 3b). The $D(Ce^{3+})$ increase, i.e., the ceria reduction, was observed to be similar for CeO_2 and $CeO_{1.9}$ substrates, so this effect depends neither on the initial Ce^{3+} ion nor on the OH group surface concentration, and most likely, it is connected with the histidine−ceria bonding. Moreover, the slope of the linear fit of the $D(Ce^{3+})$ data is lower for the reduced surface, demonstrating that reduction is less in this case. It worth mentioning that no decrease in $D(Ce^{4+})$ intensity was observed during thermal treatment, so we can exclude oxygen loss from the surface in any form. This is in agreement with our conclusion on mutual charge exchange between IM ring orbitals and Ce valence orbitals which is more pronounced on the stoichiometric CeO_2 surface.

CONCLUSIONS

Histidine adlayers on the ordered stoichiometric $CeO_2(111)$ and reduced $CeO_{1.9}$ thin films were investigated. The chemical state, coverage, and bonding of the molecules were studied by synchrotron radiation photoelectron spectroscopy and resonant photoelectron spectroscopy. Molecular orientation was examined by near edge X-ray absorption fine structure spectroscopy. Cu(111) was used as a reference sample for the histidine adsorption. It was shown that histidine binds to CeO_2 in anionic form His^{2-}. Three functional groups contribute to the strong bond formation: the carboxylate group, the imidazole ring, and the α-amino group. The imino nitrogen atom of the IM ring, carboxylic oxygen atoms, and α-amino nitrogen interact with the cerium oxide surface right after deposition. The deprotonation of the IM amino nitrogen was shown to depend on the concentration of the Ce^{4+} cations on the surface and was thermally induced. For 1 ML His/CeO_2, the imidazole ring was shown to be almost parallel to the surface. Mutual charge transfer between the histidine molecule and the oxide was observed, which was connected with the increase of the Ce^{3+} centers on the CeO_2 surface.

The effect of surface defects on the histidine adsorption was followed on the partially reduced ceria surface. Apart from disordered histidine overlayer formation, only a small difference in the deprotonation of the amino nitrogen of the imidazole ring was observed.

Heating of histidine overlayers on the cerium oxide or on Cu(111) surfaces results in molecular decomposition and partial desorption starting from 200 °C. It was shown that the stability of histidine on the oxide is much higher than that on the copper surface.

ASSOCIATED CONTENT

Supporting Information

An example of the Ce 3d core level spectra of the stoichiometric CeO_2/Cu(111) oxide before and after histidine adsorption and subsequent annealing is given in Figure S1. The original valence band spectra of samples after flashing to 100 °C are shown in Figure S2. This material is available free of charge via the Internet at http://pubs.acs.org.

AUTHOR INFORMATION

Notes

The authors declare no competing financial interest.

ACKNOWLEDGMENTS

The Materials Science Beamline is supported by the Ministry of Education of Czech Republic under Grant No. LG12003. We gratefully acknowledge the assistance of our colleagues at Elettra for providing good quality synchrotron light. The author D.M. acknowledges the support from the UNiversity research CEntre (UNCE) project no. 204023 of the Charles University in Prague. We thank V. Feyer and Y. Lykhach for helpful discussions and T. Skála for technical assistance.

REFERENCES

(1) El-Ansary, A.; Faddah, L. M. Nanoparticles as Biochemical Sensors. *Nanotechnol., Sci. Appl.* **2010**, *3*, 65−76.

(2) Solanki, P. R.; Kaushik, A.; Agrawal, V. V.; Malholta, B. D. Nanostructured Metal Oxide-Based Biosensors. *NPG Asia Mater.* **2011**, *3*, 17−24.

(3) Rahman, M. M.; Ahammad, A. J. S.; Jin, J.-H.; Ahn, S. J.; Lee, J.-J. A Comprehensive Review of Glucose Biosensors Based on Nanostructured Metal-Oxides. *Sensors* **2010**, *10*, 4855−4886.

(4) Trovarelli, A. *Catalysis by Ceria and Related Materials*; Imperial College Press: London, 2002.

(5) Vayssilov, G. N.; Lykhach, Y.; Migani, A.; Staudt, T.; Petrova, G. P.; Tsud, N.; Skála, T.; Bruix, A.; Illas, F.; Prince, K. C.; et al. Support Nanostructure Boosts Oxygen Transfer to Catalytically Active Platinum Nanoparticles. *Nat. Mater.* **2011**, *10*, 310−315.

(6) Tsud, N.; Skála, T.; Mašek, K.; Hanyš, P.; Takahashi, M.; Suga, H.; Mori, T.; Yoshikawa, H.; Yoshitake, M.; Kobayashi, K.; et al. Photoemission Study of the Tin Doped Cerium Oxide Thin Films Prepared by RF Magnetron Sputtering. *Thin Solid Films* **2010**, *518*, 2206−2209.

(7) Lykhach, Y.; Staudt, T.; Tsud, N.; Skála, T.; Prince, K. C.; Matolín, V.; Libuda, J. Enhanced Reactivity of Pt Nanoparticles Supported on Ceria Thin Films During Ethylene Dehydrogenation. *Phys. Chem. Chem. Phys.* **2011**, *13*, 253−261.

(8) Lykhach, Y.; Staudt, T.; Lorenz, M. P. A.; Streber, R.; Bayer, A.; Steinrück, H.-P.; Libuda, J. Microscopic Insights into Methane Activation and Related Processes on Pt/Ceria Model Catalysts. *ChemPhysChem* **2010**, *11*, 1496−1504.

(9) Staudt, T.; Lykhach, Y.; Tsud, N.; Skála, T.; Prince, K. C.; Matolín, V.; Libuda, J. Ceria Reoxidation by CO_2: a Model Study. *J. Catal.* **2010**, *275*, 181−185.

(10) Matolín, V.; Johánek, V.; Škoda, M.; Tsud, N.; Prince, K. C.; Skála, T.; Matolínová, I. Methanol Adsorption and Decomposition on Pt/CeO_2(111)/Cu(111) Thin Film Model Catalyst. *Langmuir* **2010**, *26*, 13333−13341.

(11) Skála, T.; Tsud, N.; Prince, K. C.; Matolín, V. Formation of Alumina−Ceria Mixed Oxide in Model Systems. *Appl. Surf. Sci.* **2011**, *257*, 3682−3687.

(12) Dvořák, F.; Stetsovych, O.; Steger, M.; Cherradi, E.; Matolínová, I.; Tsud, N.; Škoda, M.; Skála, T.; Mysliveček, J.; Matolín, V. Adjusting

Morphology and Surface Reduction of CeO_2(111) Thin Films on Cu(111). *J. Phys. Chem. C* **2011**, *115*, 7496−7503.
(13) Mani, G.; Johnson, D. M.; Marton, D.; Feldman, M. D.; Patel, D.; Ayon, A. A.; Agrawal, C. M. Drug Delivery from Gold and Titanium Surfaces Using Self-Assembled Monolayers. *Biomaterials* **2008**, *29*, 4561−4573.
(14) Hirst, S. M.; Karakoti, A.; Singh, S.; Self, W.; Tyler, R.; Seal, S.; Reilly, C. M. Bio-Distribution and *in vivo* Antioxidant Effects of Cerium Oxide Nanoparticles in Mice. *Environ. Toxicol.* **2013**, *28*, 107−118.
(15) Hirst, S. M.; Karakoti, A. S.; Tyler, R. D.; Sriranganathan, N.; Seal, S.; Reilly, C. M. Anti-Inflammatory Properties of Cerium Oxide Nanoparticles. *Small* **2009**, *5*, 2848−2856.
(16) Celardo, I.; Pedersen, J. Z.; Traversa, E.; Ghibelli, L. Pharmacological Potential of Cerium Oxide Nanoparticles. *Nanoscale* **2011**, *3*, 1411−1420.
(17) Celardo, I.; De Nicola, M.; Mandoli, C.; Pedersen, J. Z.; Traversa, E.; Ghibelli, L. Ce^{3+} Ions Determine Redox-Dependent Anti-Apoptotic Effect of Cerium Oxide Nanoparticles. *ACS Nano* **2011**, *5*, 4537−4549.
(18) Marti, E. M.; Methivier, Ch.; Dubot, P.; Pradier, C. M. Adsorption of (*S*)-Histidine on Cu(110) and Oxygen-Covered Cu(110), a Combined Fourier Transform Reflection Absorption Infrared Spectroscopy and Force Field Calculation Study. *J. Phys. Chem. B* **2003**, *107*, 10785−10792.
(19) Feyer, V.; Plekan, O.; Tsud, N.; Cháb, V.; Matolín, V.; Prince, K. C. Adsorption of Histidine and Histidine-Containing Peptides on Au(111). *Langmuir* **2010**, *26*, 8606−8613.
(20) Feyer, V.; Plekan, O.; Skála, T.; Cháb, V.; Matolín, V.; Prince, K. C. The Electronic Structure and Adsorption Geometry of L-Histidine on Cu(110). *J. Phys. Chem. B* **2008**, *112*, 13655−13660.
(21) Feyer, V.; Plekan, O.; Ptasińska, S.; Iakhnenko, M.; Tsud, N.; Prince, K. C. Adsorption of Histidine and a Histidine Tripeptide on Au(111) and Au(110) from Acidic Solution. *J. Phys. Chem. C* **2012**, *116*, 22960−22966.
(22) Xu, Z.; Yuan, S.-L.; Yan, H.; Liu, C.-B. Adsorption of Histidine and Histidine-Containing Peptides on Au(111): a Molecular Dynamics Study. *Colloids Surf., A* **2011**, *380*, 135−142.
(23) Zubavichus, Y.; Zharnikov, M.; Yang, Y.; Fuchs, O.; Heske, C.; Umbach, E.; Tzvetkov, G.; Netzer, F. P.; Grunze, M. Surface Chemistry of Ultrathin Films of Histidine on Gold as Probed by High-Resolution Synchrotron Photoemission. *J. Phys. Chem. B* **2005**, *109*, 884−891.
(24) Fleming, G. J.; Adib, K.; Rodriguez, J. A.; Barteau, M. A.; White, J. M.; Idriss, H. The Adsorption and Reactions of the Amino Acid Proline on Rutile TiO_2(110) Surfaces. *Surf. Sci.* **2008**, *602*, 2029−2038.
(25) Wilson, J. N.; Dowler, R. M.; Idriss, H. Adsorption and Reaction of Glycine on the Rutile TiO_2(011) Single Crystal Surface. *Surf. Sci.* **2011**, *605*, 206−213.
(26) Ataman, E.; Isvoranu, C.; Knudsen, J.; Schulte, K.; Andersen, J. N.; Schnadt, J. Adsorption of L-Cysteine on Rutile TiO_2(110). *Surf. Sci.* **2011**, *605*, 179−186.
(27) Gao, Y. K.; Traeger, F.; Shekhah, O.; Idriss, H.; Wöll, C. Probing the Interaction of the Amino Acid Alanine with the Surface of ZnO(10−10). *J. Colloid Interface Sci.* **2009**, *338*, 16−21.
(28) Stetsovych, V.; Pagliuca, F.; Dvořák, F.; Duchoň, T.; Vorokhta, M.; Aulická, M.; Lachnitt, J.; Schernich, S.; Matolínová, I.; Veltruská, K.; et al. Epitaxial Cubic Ce2O3 Films via Ce−CeO2 Interfacial Reaction. *J. Phys. Chem. Lett.* **2013**, *4*, 866−871.
(29) http://www.kolibrik.net/science/kolxpd/.
(30) Briggs, D.; Seah, M. P. *Practical Surface Analysis*, 2nd ed.; John Wiley & Sons Ltd: 1990; Vol. *1*, Auger and X-ray Photoelectron Spectroscopy.
(31) http://www.chemspider.com.
(32) Zubavichus, Y.; Shaporenko, A.; Grunze, M.; Zharnikov, M. Innershell Absorption Spectroscopy of Amino Acids at All Relevant Absorption Edges. *J. Phys. Chem. A* **2005**, *109*, 6998−7000.
(33) Carravetta, V.; Plashkevych, O.; Ågren, H. A Theoretical Study of the Near-Edge X-ray Absorption Spectra of Some Larger Amino Acids. *J. Chem. Phys.* **1998**, *109*, 1456−1464.
(34) Apen, E.; Hitchcock, A. P.; Gland, J. L. Experimental Studies of the Core Excitation of Imidazole, 4,5-Dicyanoimidazole, and s-Triazine. *J. Phys. Chem.* **1993**, *97*, 6859−6866.
(35) Kaznacheyev, K.; Osanna, A.; Jacobsen, C.; Plashkevych, O.; Vahtras, O.; Ågren, H.; Carravetta, V.; Hitchcock, A. P. Innershell Absorption Spectroscopy of Amino Acids. *J. Phys. Chem. A* **2002**, *106*, 3153−3168.
(36) Taylor, J. B.; Mayor, L. C.; Swarbrick, J. C.; O'Shea, J. N.; Schnadt, J. Charge-Transfer Dynamics at Model Metal-Organic Solar Cell Surfaces. *J. Phys. Chem. C* **2007**, *111*, 16646−16655.
(37) Lykhach, Y.; Johánek, V.; Aleksandrov, H. A.; Kozlov, S. M.; Happel, M.; Skála, T.; Petkov, P., St.; Tsud, N.; Vayssilov, G. N.; Prince, K. C.; et al. Water Chemistry on Model Ceria and Pt/Ceria Catalysts. *J. Phys. Chem. C* **2012**, *116*, 12103−12113.
(38) Feyer, V.; Plekan, O.; Tsud, N.; Lyamayev, V.; Cháb, V.; Matolín, V.; Prince, K. C; Carravetta, V. Adsorption Structure of Glycyl-Glycine on Cu(110). *J. Phys. Chem. C* **2010**, *114*, 10922−10931.
(39) Zhang, W.; Carravetta, V.; Plekan, O.; Feyer, V.; Richter, R.; Coreno, M.; Prince, K. C. Electronic Structure of Aromatic Amino Acids Studied by Soft X-ray Spectroscopy. *J. Chem. Phys.* **2009**, *131*, 35103−35114.
(40) Wickrama Arachchilage, A. P.; Wang, F.; Feyer, V.; Plekan, O.; Prince, K. C. Photoelectron Spectra and Structures of Three Cyclic Dipeptides: PhePhe, TyrPro, and HisGly. *J. Chem. Phys.* **2012**, *136*, 124301−124309.
(41) Matolín, V.; Matolínová, I.; Dvořák, F.; Johánek, V.; Mysliveček, J.; Prince, K. C.; Skála, T.; Stetsovych, O.; Tsud, N.; Václavů, M.; et al. Water Interaction with CeO_2(111)/Cu(111) Model Catalyst Surface. *Catal. Today* **2012**, *181*, 124−132.